[Journal of Geophysical Research: Planets]

Supporting Information for

[Tectonism and Enhanced Cryovolcanic Potential Around a Loaded Sputnik Planitia Basin, Pluto]

[Patrick J. McGovern[1], Oliver L. White[2,3], Paul M. Schenk[1]]

[[1]Lunar and Planetary Institute, Universities Space Research Association, Houston, TX, 77058; [2]SETI Institute, Mountain View, CA, 94043; [3]NASA Ames Research Center, Moffett Field, CA, 94035]

Contents of this file

Additional Supporting Information (Files uploaded separately)

Caption for Dataset S1

Introduction

The Supporting Information includes Text S1 and S2, which respectively describe the concept behind the FEM Model Grids used in our simulations (accompanied by Figures S1 and S2 that show the entirety and a detail of the model domain) and the justification behind our treatment of initial basin topography as uncompensated in our modeling (accompanied by Figures S3 and S4 that respectively show the difference in final basin floor topography for nominal and compensated models, and the modeled state of stress for compensated basin topography). We also include Dataset 1, which is a zipped folder containing the ArcGIS shape files (as well as auxiliary files) for the mapping of Pluto's tectonism presented in Fig. 2 of the

Text S1: FEM Model Grids

The Finite Element Method (FEM) discretizes the modeled domain into numerous contiguous "elements" that facilitate the solution of partial differential equations via

matrix techniques. Figure S1 shows the extent of the model domain, anchored on the symmetry axis at radial coordinate value $r = 0$ (using the first definition of "radius" defined in the *Coordinate Systems* sub-section above). Individual elements (of order a km or so in width) are too small to be resolved at the scale of this figure. Figure S2 shows a close up of the model domain near the location of the modeled basin. Individual elements can be distinguished in this figure, giving an impression of the resolution of the model and the scale of the overall calculation.

Text S2: Models with Initially Compensated Topography

The models presented above have initial basin topography that is uncompensated. Thus, there is no topographic relief at the base of any model domain, i.e., the model shells are unaltered at its base. This is a consequence of the distinction between the full shell thickness (comprising both shallow elastic and deep ductile ice components) and the modeled shell (containing only the former). The models only contain the elastic part of Pluto's ice shell. Many estimates of Pluto's ice shell thickness exceed 150 km; under such conditions, the compensating relief on the shell base would occur entirely within the ductile layer, which is the main reason why the models presented above (lacking the deep ductile shell) are uncompensated. Note also that if the elastic part comprised the entire thickness of Pluto's ice shell, the extremely low density contrast between water ice and liquid water, for initial basin depths greater than a few kilometers, would reduce the compensated shell thickness to zero, rendering the models useless.

The lack of compensation of the initial surface mass deficit from the basin topography induces a small upward deflection of the shell. In practice, this uplift is overwhelmed by the subsidence induced by the N_2 ice load. Nonetheless, it is important to quantify this effect by an explicit accounting for a compensating load that negates the upward deflection of the uncompensated shell. We accomplish this by adding an extra boundary force term to the shell basal boundary condition, of magnitude $(\rho_o - \rho_{ice})*g*H(r)*f_c$, where ρ_o and ρ_{ice} are the densities of the ocean and ice shell, respectively, g is Pluto's gravitational acceleration, $H(r)$ is the basin topography function defined above, and f_c is a scaling constant that is iteratively adjusted to minimize the displacement of the basin surface caused by the absence of compensation. In practice, for values of $f_c \approx 0.75$, such displacements are order several meters (fractions of a percent of the basin topography). See Hemingway and Matsuyama (2017) for a discussion of isostatic equilibrium in spherical coordinates.

For the nominal model parameters (e.g., as in the uncompensated model of Figure 5), the difference between uncompensated and compensated surface deflections is a maximum of about 900 m at the basin center, $r_p = 0$ km (dashed and solid thin red lines in Figure S3, respectively). This increases load volume by several percent, which has a small effect on the resulting stress states. Surface stress magnitudes for the compensated model are slightly larger for the compensated model vs. the uncompensated one (compare Figure S4A with Fig. 5B). The predicted depth and radial extent of the failure zone are also slightly increased by adding compensation (compare

Figure S4B with Fig. 5B). A similar effect is seen for the effective buoyant density calculation (Figure S4C and Fig. 5C). None of these changes are large enough to significantly affect our conclusions regarding the T_e of Pluto's ice shell or the configuration (shape and depth) of the initial Sputnik basin.

Reference:

Hemingway, D. J., and I. Matsuyama (2017), Isostatic equilibrium in spherical coordinates and implications for crustal thickness on the Moon, Mars, Enceladus, and elsewhere, *Geophys. Res. Lett., 44*, 7695–7705, doi:10.1002/ 2017GL073334.

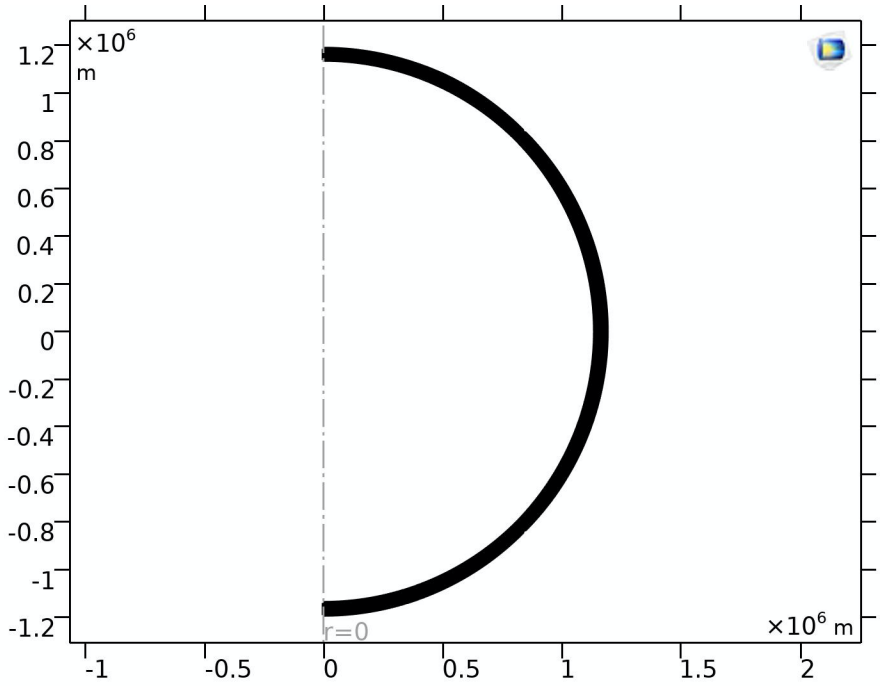

Figure S1. Entire geometry of the spherical shell finite element grid for the nominal model (T_e = 50 km) of Pluto's ice elastic lithosphere around SP. Individual elements are not visible at this resolution.

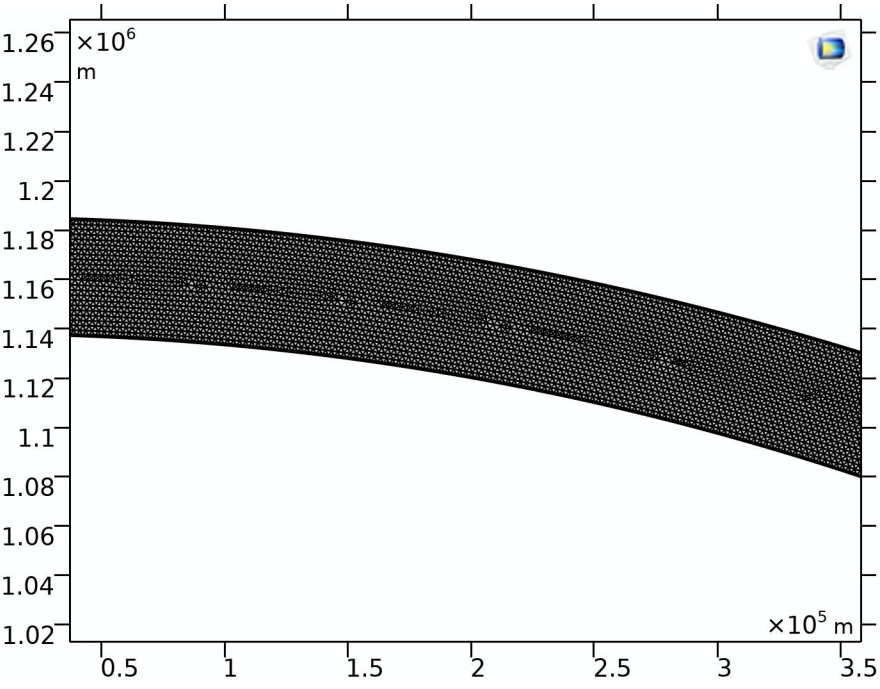

Figure S2. Close up of the model of Figure S1 near the symmetry axis at the location of the model basin.

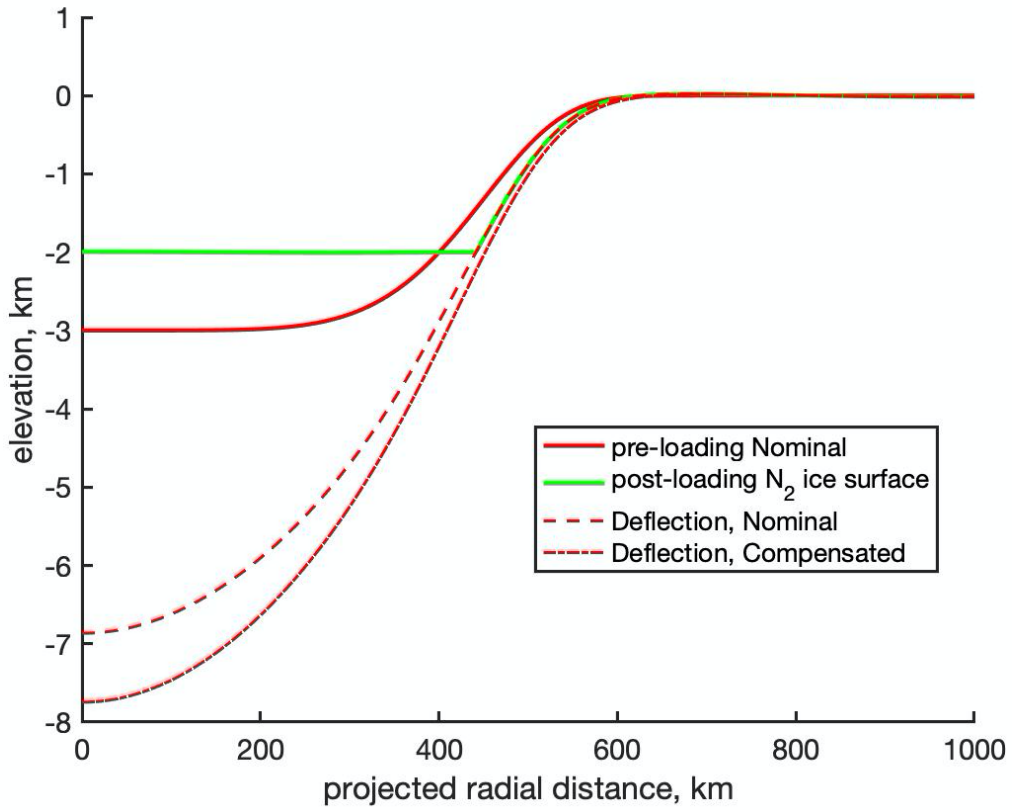

Figure S3. Comparison of final basin floor topography, as in Figure 13A, for nominal model (model of Figure 5, dashed thin red line) and an otherwise nominal model with compensation for the basin topography (solid thin red line).

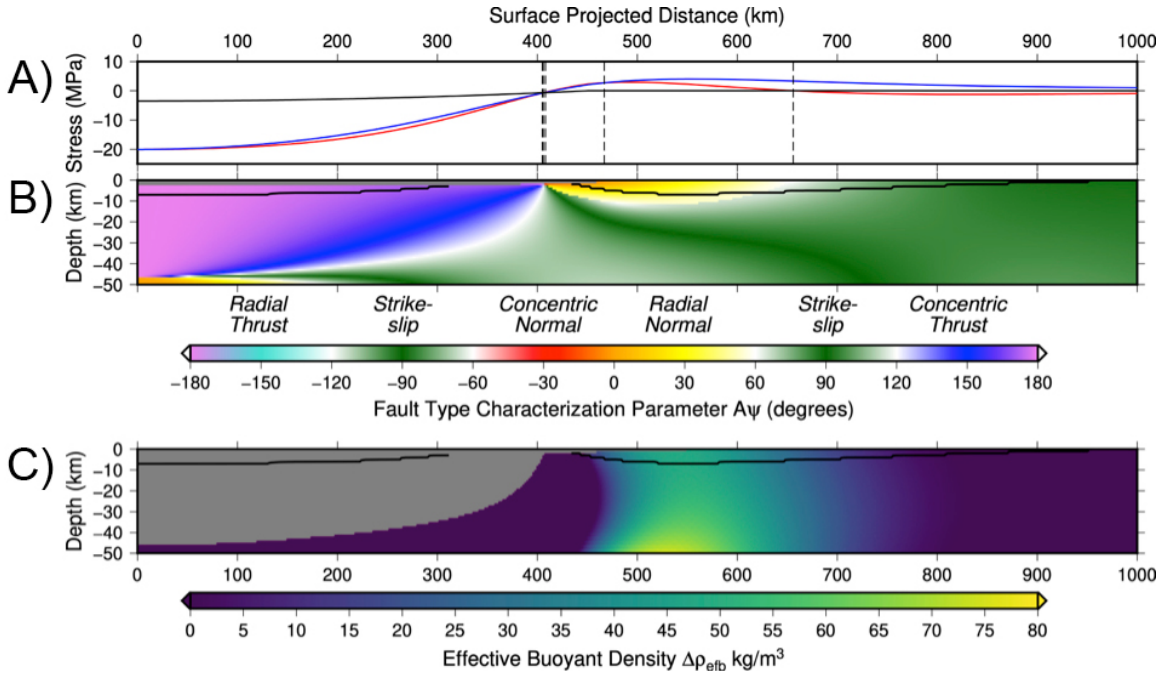

Figure S4. Surface horizontal normal stresses, stress regimes, and effective buoyant density, as in Figure 5, for an otherwise nominal model with compensation for the basin topography.

Data Set S1. The tectonics mapping presented in Fig. 2 was performed in ArcMap 10.3.1, and we include the ArcGIS shape files and auxiliary files for the eight mapped tectonic systems, plus the depressions of the ridge-trough system, in a zipped folder included with the Supplementary Material entitled "ds01.zip". The files are named according to each system as shown in the legend of Fig. 2, and the shape files (.shp extension) can be read into ArcGIS or the free-to-download QGIS software. The base maps we used for mapping include the LORRI-MVIC global mosaic and the global stereo digital elevation model of Pluto, both projected at 300 m/pixel. These are archived in the PDS Imaging and Cartography Node, and can be downloaded at the following links:

Global mosaic:
https://astrogeology.usgs.gov/search/map/Pluto/NewHorizons/Pluto_NewHorizons_Global_Mosaic_300m_Jul2017

Global DEM:
https://astrogeology.usgs.gov/search/map/Pluto/NewHorizons/Pluto_NewHorizons_Global_DEM_300m_Jul2017